NANO · MICRO small
www.small-journal.com

Nanopore-Based, Rapid Characterization of Individual Amyloid Particles in Solution: Concepts, Challenges, and Prospects

*Jared Houghtaling, Jonathan List, and Michael Mayer**

Aggregates of misfolded proteins are associated with several devastating neurodegenerative diseases. These so-called amyloids are therefore explored as biomarkers for the diagnosis of dementia and other disorders, as well as for monitoring disease progression and assessment of the efficacy of therapeutic interventions. Quantification and characterization of amyloids as biomarkers is particularly demanding because the same amyloid-forming protein can exist in different states of assembly, ranging from nanometer-sized monomers to micrometer-long fibrils that interchange dynamically both in vivo and in samples from body fluids ex vivo. Soluble oligomeric amyloid aggregates, in particular, are associated with neurotoxic effects, and their molecular organization, size, and shape appear to determine their toxicity. This concept article proposes that the emerging field of nanopore-based analytics on a single molecule and single aggregate level holds the potential to account for the heterogeneity of amyloid samples and to characterize these particles—rapidly, label-free, and in aqueous solution—with regard to their size, shape, and abundance. The article describes the concept of nanopore-based resistive pulse sensing, reviews previous work in amyloid analysis, and discusses limitations and challenges that will need to be overcome to realize the full potential of amyloid characterization on a single-particle level.

1. Introduction

Neurodegenerative disorders like Alzheimer's disease and Parkinson's disease, as well as other medical conditions like Type II diabetes, are associated with the presence and activity of toxic protein aggregates known as amyloids (**Table 1**).[1–6] The incidence, or probability of occurrence, of many of these diseases increases with age.[5] Today, more than 30 million people worldwide suffer from dementias linked to amyloids, and the World Health Organization predicts that this figure may exceed 100 million by the year 2050 as life expectancies increase.[7] While these conditions are devastating with regard to patient suffering and impacts on family members and caregivers, neurological amyloidoses are also responsible for more than USD 500 billion in worldwide annual costs.[7] Research groups across scientific disciplines have therefore investigated strategies to better understand and interfere with the transition from soluble monomeric proteins and peptides into soluble oligomers and, eventually, into insoluble amyloid fibrils and plaques that are hallmarks of several neurodegenerative diseases.[8,9]

Amyloid-forming proteins often undergo an aggregation process analogous to crystal formation where the generation of a "seed" is the rate-limiting step for the assembly of a large ordered structure.[10,11] Treatments that are currently in clinical trial target these seeds and their precursors in order to redirect or disrupt downstream aggregate formation at an early stage before irreversible nerve cell damage occurs.[12] Additionally, there is evidence that the size, shape, and concentration of oligomeric amyloid aggregates determine their toxicity to neurons,[13,14] and patients with certain amyloidoses have elevated counts of these oligomeric species in their cerebrospinal fluid (CSF).[15,16] Findings like these suggest that soluble amyloid aggregates may be valuable biomarkers for predicting or monitoring disease progression and may also help to assess the efficacy of therapeutic intervention. There is thus a need for a characterization technique that provides a comprehensive profile of the individual amyloid particles in bodily fluids like CSF, blood, tears, saliva, or urine.[17,18]

While a range of techniques is currently being used to characterize amyloids and their aggregation processes (**Table 2**), amyloid samples remain extremely difficult to analyze and none of the established techniques meets all demands of an ideal analysis method as outlined in **Table 3**.[19,20,25] For instance, amyloid aggregates are challenging analytes to characterize because they are heterogeneous in size and structure, they rearrange, interchange dynamically and grow over time, and they adhere to various surfaces including tubing and microvials.[26,27] Methods attempting to characterize ensembles of these heterogeneous

J. Houghtaling
Department of Biomedical Engineering
University of Michigan
Ann Arbor, MI 48109, USA
J. Houghtaling, Dr. J. List, Prof. M. Mayer
Adolphe Merkle Institute
University of Fribourg
Chemin des Verdiers 4 CH-1700, Fribourg, Switzerland
E-mail: michael.mayer@unifr.ch
The ORCID identification number(s) for the author(s) of this article can be found under https://doi.org/10.1002/smll.201802412.

DOI: 10.1002/smll.201802412

 © 2018 WILEY-VCH Verlag GmbH & Co. KGaA, Weinheim

aggregates obscure potentially important physical differences between individual macromolecular assemblies.[28] Conversely, techniques that label or chemically modify individual amyloids vary in their sensitivity and specificity to different morphologies or chemical structures and the modification itself may alter the sample.[29] Long and extensive sample preparation processes can bias amyloid populations toward stable species and may destroy potentially important transient complexes.[22] Nonetheless, current approaches to characterize amyloids provide a range of relevant parameters of amyloid aggregates. For instance, methods like transmission electron microscopy (TEM), atomic force microscopy (AFM), and mass spectrometry (MS) create "macromolecular snapshots," providing structural information about proteins and aggregates at a single time point.[20] Other techniques using fluorescent dyes, tracer molecules such as ^{18}F-florbetapir, or fluorescently labeled antibodies track aggregation processes in vivo or in vitro to probe the dynamics and formation rates of different complexes.[30] Some methods focus on defining and detecting amyloid biomarkers that indicate disease predisposition or progression.[15] Sometimes, researchers perform various analysis approaches in parallel in order to determine structural and chemical characteristics of an amyloid sample, though such combinations often require significant financial and technical resources as well as expertise. An ideal technique for amyloid characterization would combine these functionalities to provide rich, rapid, and robust information about single amyloid particles in high-throughput and in a clinical setting without the need for expensive equipment or technical expertise (Table 3).

One emerging technique that may meet several of these demands is resistive pulse-based nanopore sensing, as it is capable of characterizing individual unlabeled particles in aqueous solution. The method was originally developed in the late 1940s for applications on the microscale such as counting and characterizing biological cells.[31–33] Resistive pulse experiments have now made it possible to probe nanoscale analytes including small molecules,[34,35] metal ions,[36] polynucleotides,[37] nanoparticles,[38,39] proteins,[40–43] and amyloids.[42,44–56] The application of resistive pulse sensing to protein characterization emerged less than 15 years ago and is not as developed as the established methods listed in Table 2, but it combines attractive capabilities that make it a potentially powerful tool for studying amyloids. Some of these benefits, such as the characterization of shapes, volumes, diffusion coefficients, and electrical and mechanical properties of individual proteins and protein complexes, are appealing for fundamental biophysical studies. Other advantages, including the ability to extract resistive pulses from single unlabeled molecules and to perform analyses of those resistive pulses in real time, may be clinically useful.[57] This article focuses specifically on the application of resistive pulse sensing to amyloid-related protein analytes and discusses the concepts and challenges of this application.

2. Principles of Resistive Pulse Sensing

The concept of resistive pulse sensing traces back to the invention of the Coulter counter for blood cells.[58] Briefly, if two electrolyte-filled reservoirs are connected by a small channel, a difference in electrical potential between the two reservoirs generates a current

Jared Houghtaling is a Ph.D. student in the Department of Biomedical Engineering at the University of Michigan (Ann Arbor), and he is conducting his thesis research under the direction of Prof. Michael Mayer in the Adolphe Merkle Institute at the University of Fribourg. He received his undergraduate degree in 2014 from the Department of Bioengineering at the University of Washington (Seattle). His research aims to improve nanopore-based protein characterization by developing novel experimental and analytical techniques, with the ultimate goal of applying these new methods to detect and investigate medically relevant protein targets like amyloids.

Jonathan List received his Ph.D. in physics in 2018 from the Technical University Munich in the group of Prof. Friedrich Simmel. He is currently working as a postdoctoral researcher in the Adolphe Merkle Institute at the University of Fribourg under the direction of Prof. Michael Mayer. His recent research focuses on applying single-molecule techniques to detect and characterize amyloid species and to investigate the aggregation kinetics of amyloid particles ex vivo. He also engages in the development and design of self-assembled, DNA-based nanostructures and devices.

Michael Mayer obtained a Ph.D. in biophysical chemistry with Horst Vogel at the Swiss Federal Institute of Technology in Lausanne (EPFL), followed by postdoctoral research with George M. Whitesides at Harvard University. From 2004 to 2015, he was a faculty member in Biomedical Engineering at the University of Michigan (Ann Arbor). In the fall of 2015, his group moved to the Adolphe Merkle Institute at the University of Fribourg, where he holds the chair of Biophysics. His research takes inspiration from nature to solve problems in biophysics ranging from detecting single protein complexes and characterizing transporter proteins to engineering biocompatible electrical power sources.

© 2018 WILEY-VCH Verlag GmbH & Co. KGaA, Weinheim

Table 1. Peptides and proteins that form amyloid aggregates in human disease. Several of these amyloids have yet to be thoroughly characterized with respect to structure.

Name of peptide or protein	Number of amino acids[a)]	Secondary structure[b)]	Associated diseases	Relative global prevalence[c)]	Number of biomarker publications[d)]
Amyloid-β peptide (Aβ)	37–43	Intrinsically disordered	Alzheimer's disease Hereditary cerebral hemorrhage with amyloidosis	Common	1284
α-Synuclein (α-Syn)	140	Intrinsically disordered	Parkinson's disease (with/without dementia) Dementia with Lewy bodies Multiple system atrophy	Common	139
Prion protein (PrP)	208	Intrinsically disordered (1–102), all α-helix, prion-like (103–208)	Creutzfeldt-Jakob disease Fatal insomnia Gerstmann-Sträussler-Scheinker disease Huntington disease–like 1 Spongiform encephalopathy New variant Creutzfeldt-Jakob disease Kuru Hereditary sensory and autonomic neuropathy	Very rare	26
Microtubule-associated protein tau (τ)	352–441	Intrinsically disordered	Alzheimer's disease Pick disease Progressive supranuclear palsy Corticobasal degeneration Frontotemporal dementia w parkinsonism linked to chr17 Argyrophilic grain disease Tangle predominant dementia Guam Parkinson dementia complex Frontotemporal lobar degeneration Chronic traumatic encephalopathy Ganglioglioma Meningioangiomatosis Subacute sclerosing panencephalitis Lead encephalopathy Tuberous sclerosis Hallervorden-Spatz disease Lipofuscinosis	Common	1018
Huntingtin exon 1	≈103–187	Intrinsically disordered	Huntington disease	Moderate	15
Abri peptide	34	Intrinsically disordered	Familial British dementia	Very rare	0
Adan peptide	34	Intrinsically disordered	Familial Danish dementia	Very rare	0
Fragments of immunoglobulin light chains	≈100	All β-sheet, Ig-like	Light-chain amyloidosis	Rare	3
Fragments of immunoglobulin heavy chains	≈190	All β-sheet, Ig-like	Heavy-chain amyloidosis (renal)	Rare	0
Full or N-term fragments of serum amyloid A protein (SAA)	45–104	All-α, SAA-like four-helix bundle	AA amyloidosis	Rare	452
Transthyretin (TTR)	127	All β-sheet, prealbumin-like	Senile systemic amyloiosis Familial amyloidotic polyneuropathy Familial amyloid cardiomyopathy Leptomeningeal amyloidosis	Rare	53
β2-microglobulin (β2-m)	99	All β-sheet, Ig-like	Dialysis-related amyloidosis Hereditary visceral amyloidosis	Rare	8
N-term fragments of apolipoprotein A-I (ApoAI)	69–100	Intrinsically disordered	ApoAI amyloidosis	Rare	14
C-term extended apolipoprotein A-II (ApoAII)	98	Unknown	ApoAII amyloidosis (renal)	Rare	2
N-term fragments of apolipoprotein A-IV (ApoAIV)	≈70	Unknown	ApoAIV amyloidosis	Rare	3
Apolipoprotein C-II (ApoCII)	79	All α-helix, unknown fold	ApoCII amyloidosis (renal)	Rare	0
Apolipoprotein C-III (ApoCIII)	79	All α-helix, unknown fold	ApoCIII amyloidosis (renal)	Rare	3
Fragments of gelsolin	53 or 71	Intrinsically disordered	Familial amyloidosis, Finnish type	Very rare	6

© 2018 WILEY-VCH Verlag GmbH & Co. KGaA, Weinheim

Table 1. Continued.

Name of peptide or protein	Number of amino acids[a)]	Secondary structure[b)]	Associated diseases	Relative global prevalence[c)]	Number of biomarker publications[d)]
Lysozyme (LYS)	130	α-helix + β-sheet, lysozyme fold	Lysozyme amyloidosis (visceral)	Rare	8
Fragments of fibrinogen α-chain	45–81	Unknown	Fibrinogin amyloidosis (renal)	Rare	27
N-term truncated cystatin C	110	α-helix + β-sheet, cystatin-like	Hereditary cerebral hemorrhage with amyloidosis, Icelandic type	Very rare	21
Islet amyloid polypeptide (IAPP)	37	Intrinsically disordered	Type II diabetes Insulinoma	Common	8
Calcitonin	32	Intrinsically disordered	Medullary carcinoma of the thyroid	Moderate	0
Atrial natriuretic factor (ANF)	28	Intrinsically disordered	Atrial amyloidosis	Common	0
N-term fragments of prolactin (PRL)	34	Unknown	Pituitary prolactinoma	Moderate	2
Insulin	(30 + 21)	All α-helix, insulin-like	Injection-localized amyloidosis	Very rare	61
Medin	50	Intrinsically disordered	Aortic medial amyloidosis	Rare	0
Lactotransferrin (lactoferrin)	691	α-helix + β-sheet, periplasmic binding protein-like II	Gelatinous drop-like corneal dystrophy	Rare	1
Odontogenic ameloblast-associated protein (ODAM)	110–118	Unknown	Calcifying epithelial odontogenic tumors	Rare	1
Pulmonary surfactant-associated protein (SP-C)	35	All α-helix, transmembrane helical fragment	Pulmonary alveolar proteinosis	Rare	1
Leukocyte cell-derived chemotaxin-2	133	All β-sheet, barrel-sandwich hybrid	Renal amyloidosis	Rare	0
Galectin 7 (Gal-7)	136	All β-sheet, concanavalin A-like lectins	Lichen amyloidosis, macular amyloidosis	Rare	0
Corneodesmosin (CDSN)	167, 182, 206	Intrinsically disordered	Hypotrichosis simplex of the scalp	Very rare	0
C-term fragments of kerato-epithelin (βig-h3)	50–200	Unknown	Lattice corneal dystrophy, type 1 Lattice corneal dystrophy, type 3A Lattice corneal dystrophy, Avellino type	Common	0
Semenogelin-1 (SGI)	439	Unknown	Seminal vesicle amyloidosis	Moderate	0
Protein S100A8/A9	92 or 113	All α-helix, EF hand-like	Prostate cancer	Common	8
Enfuvirtide	36	Unknown	Injection-localized amyloidosis	Very rare	0

[a)]The total number of amino acids corresponds to the protein or peptide species that forms amyloids; [b)]Secondary structures are determined from the Structural Classification of Proteins (SCOP) database; [c)]Estimates of relative global prevalence estimates are approximate and binned as follows: "Very rare" corresponds to less than 10 000 cases globally, "Rare" corresponds to a maximum of 100 000 cases globally, "Moderate" represents a maximum of one million cases globally, and "Common" represents more than one million cases globally; [d)]Numbers of publications discussing each protein or peptide as potential biomarkers were gathered via Web of Science using an advanced search to find articles containing the respective protein or peptide name AND the word "biomarker" AND the word "amyloid"; Adapted with permission.[2] Copyright 2017, Annual Reviews.

through the channel. This ionic current is constant at a constant potential difference, but when an insulating particle passes from one reservoir to the other through the channel (i.e., through the sensing volume), it transiently displaces conducting electrolyte and reduces the current to produce a resistive pulse.[38,59,60] With regard to the other macromolecules in solution, the method can also be thought of as a transient purification, as it interrogates one particle at a time from bulk solution. Due to high electric field and concomitant fast electrophoretic motion of particles in the pore, the probability of finding two macromolecules in the small sensing volume at the same time is very low, especially when the average duration between particle capture is at least 100-fold longer than the average duration of the resistive pulses. In scenarios where particle concentrations are relatively high ($\approx 1 \times 10^{-3}$ M or greater) and each particle dwells within the pore for a relatively long duration (≈1 ms or greater), the probability of multiple-occupancy events increases and may lead to rare events that must be excluded from analysis.[61] For protein analysis by resistive pulse sensing, the protein concentrations are, however, typically in the micromolar range or below and the dwell times are typically shorter than 1 ms. "Continuous" resistive-pulses, like those generated when long strands of nucleic acids pass end-to-end through a sensing volume, have a particular set of intricacies that are reviewed elsewhere.[62–67] Here, we highlight the resistive pulses produced by discrete particles, which typically have lengths shorter than the length of the nanopore, as these are relevant for the sensing and characterization of amyloid oligomers and short protofibrils.

© 2018 WILEY-VCH Verlag GmbH & Co. KGaA, Weinheim

Table 2. Comparison of different characterization techniques for amyloid samples.

Characterization technique	Type of technique				Applicable to these species of amyloid					Structural resolution					Resources Required[a]	Expertise Required[a]	Continuous Measurements[b]
	Single mol.	Correlation	Imaging	Ensemble	Monomer	Small oligo.	Large oligo.	Protofibril	Fibril	Atomic	Secondary	Tertiary and quarternary	Morphology	Assembly size distrib.			
Biological nanopores	✓				✓	✓[a]							✓	✓	*[b]	**	Y[c]
Synthetic nanopores	✓				✓	✓	✓	✓					✓	✓	*	***	Y
Ion mobility spectroscopy-mass spectroscopy (IMS-MS)[19–21]	✓				✓	✓	✓							✓	**	**	N[d]
Dynamic light scattering[20]		✓			✓	✓	✓	✓						✓	*	**	Y
Fluorescence correlation spectroscopy (FCS)		✓	✓		✓	✓	✓	✓						✓	**	***[e]	Y
(Cryo-)transmission electron microscopy			✓		✓	✓	✓	✓	✓	✓		✓	✓	✓	***	***	N
Scanning tunneling microscopy[20,21]			✓			✓	✓	✓	✓			✓	✓		***	***	N
Atomic force microscopy[19,20,23,24]			✓			✓	✓	✓	✓			✓	✓		**	***	Y
Super resolution microscopy			✓			✓	✓	✓	✓			✓	✓		**	**	Y
Birefringence[20,22]			✓						✓		✓				*	*	N
Fluorescent binders[19,20,22–24]			✓	✓				✓	✓		✓				*	*	Y
Fluorescence spectroscopy[20,22,24]				✓	✓	✓	✓	✓	✓		✓	✓			*	*	Y
Fluorescence microscopy[19,20]			✓		✓	✓	✓	✓	✓		✓	✓			*	**	Y
Solution-state NMR[19–21,24]				✓	✓	✓	✓			✓					***	***	Y
Solid-state NMR[19,20,23,24]				✓				✓	✓	✓					***	***	N
X-ray absorption spectroscopy[20]				✓	✓	✓	✓	✓	✓	✓					***	***	N
Circular dichroism spectroscopy[20,24]				✓	✓	✓	✓	✓			✓				*	**	Y
Fourier transform infrared spectroscopy[20,22–24]				✓	✓	✓	✓	✓	✓		✓				**	**	Y
Neutron scattering[20,21]				✓				✓	✓		✓				***	***	N
X-ray fiber diffraction[19,20,22–24]				✓				✓	✓		✓				***	***	N
Electron spin resonance[20]				✓	✓	✓	✓	✓	✓			✓			**	**	N
Hydrogen deuterium exchange[20]				✓	✓	✓	✓	✓	✓			✓			**	**	N
Limited proteolysis[20,21]				✓	✓	✓	✓	✓	✓			✓			**	**	N
Gel electrophoresis[19–21]				✓	✓	✓	✓							✓	*	*	N
PICUP[20,21]				✓	✓	✓	✓							✓	*	*	N
Size exclusion chromatography[19–21,24]				✓	✓	✓	✓	✓						✓	*	*	Y
Analytical ultracentrifugation[20]				✓	✓	✓	✓	✓						✓	**	**	N

[a]There is potential to characterize small oligomers using a large biological pore; [b]One star corresponds to minimal resources or expertise; [c]"Y," or yes, represents continuous measurements; [d]"N," or no, represents a snapshot measurement; [e]Three stars correspond to extensive resources or expertise. Adapted with permission.[20] Copyright 2006, John Wiley and Sons.

© 2018 WILEY-VCH Verlag GmbH & Co. KGaA, Weinheim

Table 3. Characteristics of an ideal next-generation method for characterizing amyloid aggregates and their precursors.

– Capability to characterize, quantify, and monitor amyloid monomers, amyloid oligomers, protofibrils, and fibrils on a single-molecule and single aggregate level.
– Rapid analysis within seconds and within aqueous solution.
– Label-free analysis method with minimal sample preparation such that the amyloid status of the sample remains unperturbed and representative of its status in the patient.
– Small sample volumes (microliters or smaller).
– Capability to characterize physical properties like 3D shape, volume, secondary structure, conformational change, dipole moment, and diffusion coefficients. Ideally refine the approach such that it may ultimately reveal the mass of individual amyloid particles and provide atomic-level structural information about these particles.
– Broadly accessible technique.
– High reproducibility between different users and measurement environments.
– High specificity to amyloid biomarker of interest.
– High—ideally single molecule—sensitivity to amyloid aggregates at extremely low concentrations.
– Low-cost instrumentation and operation.
– Capability to make measurements in a clinical environment with instant diagnostic value.
– Capability to detect amyloids in a range of bodily fluids like cerebrospinal fluid, tears, saliva, blood, or urine.
– Minimal technical expertise required for operation.
– Capability to detect post-translational modifications of amyloid-forming peptides and proteins such as phosphorylations or glycylations, etc.

For resistive pulse sensing at any scale, sensing volumes must be appropriately sized to their target analyte.[68] A particle will not produce a detectable signal if its volume is more than 1000-fold smaller than the sensing volume, and it will not translocate through a sensing volume that it cannot enter due to steric constraints. Particles that do not conform to these size restrictions can still provide indirect information about the system,[69] but they cannot be analyzed directly within the sensing volume. If the sensing volume is sufficiently large to allow a nonspherical particle to rotate relatively freely, the particle will produce a unique resistive pulse signature that depends not only on its volume, but also on its shape and relative orientation to the electric field (**Figure 1**).[41,68] Rotations during transit through the pore cause fluctuations within the resistive pulse that originate from different orientations of a 3D shape in the electric field. The physical basis for this orientation dependence was first explored by Golibersuch[68] and others,[31,70] who found that rotations of disk-shaped red blood cells passing through a cylindrical channel generated characteristic resistive pulses with distinct minima and maxima. The minimum values (ΔI_{MIN}) corresponded to the cell in its edgewise orientation relative to the channel axis, and the maximum values (ΔI_{MAX}), which were about twofold greater in amplitude than the minimum, corresponded to the cell in its crosswise orientation relative to the channel axis (Figure 1b). Fricke[71] and others[72] quantified these effects with a physical descriptor, the electrical shape factor γ, which depends on the particle's ellipsoidal shape and orientation within a cylindrical sensing volume, and is directly proportional to resistive pulse amplitude. The electrical shape factor is also valid on the nanoscale, though nanometer-sized proteins and particles rotate at a rate that is several orders of magnitude faster than cells and thus require high-bandwidth recording electronics and strategies like surface anchoring[40] to slow their rotation in order to fully resolve their characteristic fluctuations. Our group recently took advantage of these fluctuations in order to approximate the shape of an individual particle translocating through a nanopore.[41,73] Furthermore, we used the particle's bias toward certain orientations during its transit through the strong electric field inside of the nanopore (several MV m^{-1}) to estimate the net dipole moment of the particle. The most probable speed at which the particle transitions between these orientations is proportional to its bulk rotational diffusion coefficient, and the amount of time that a particle occupies the sensing volume, also referred to as its dwell or residence time, is a function of the particle's lateral diffusion coefficient and is inversely proportional to its net charge. Measured simultaneously, these five parameters—shape, volume, charge, rotational diffusion coefficient, and dipole moment—define a high-content multidimensional "fingerprint" of an unlabeled particle that helps to characterize, and discriminate between, particles in a mixture.[41]

Resistive pulse sensing can also probe the conformational variability of particles.[43,74,75] When a particle is sterically constrained within a small sensing volume, the resistive pulse associated with that particle's translocation provides information about the particle's conformational variability.[43,74,75] In the case of proteins, this information appears as fluctuations in amplitudes between multiple resistive pulses (Figure 1d) and has been attributed to differences in secondary structural composition (e.g., β-sheet to α-helix ratio).[43,74,75] Resistive pulse experiments, in principle, may also make it possible to monitor the interactions of particles or amyloid-forming molecules with soluble species. For instance, our group used a nanopore to monitor immunoprecipitation and to determine the binding affinity of an antibody to the surface of a virus particle by relating resistive pulse amplitudes over time to the number of binding sites occupied on the particle. In these approaches, each binding event increased the aggregate volume, and thus the magnitude of the resistive pulse, by a constant increment.[76–78] Likewise, Si and Aksimentiev showed that denatured proteins produce different resistive pulses than their native protein counterparts, and that the differences correspond to unfolding processes.[41,79] Each of these applications of resistive pulse sensing provides different information about individual particles in aqueous solution and about their time-dependent changes in response to various stimuli. **Table 4** summarizes the attributes that nanopore-based analysis can bring to amyloid characterization.

© 2018 WILEY-VCH Verlag GmbH & Co. KGaA, Weinheim

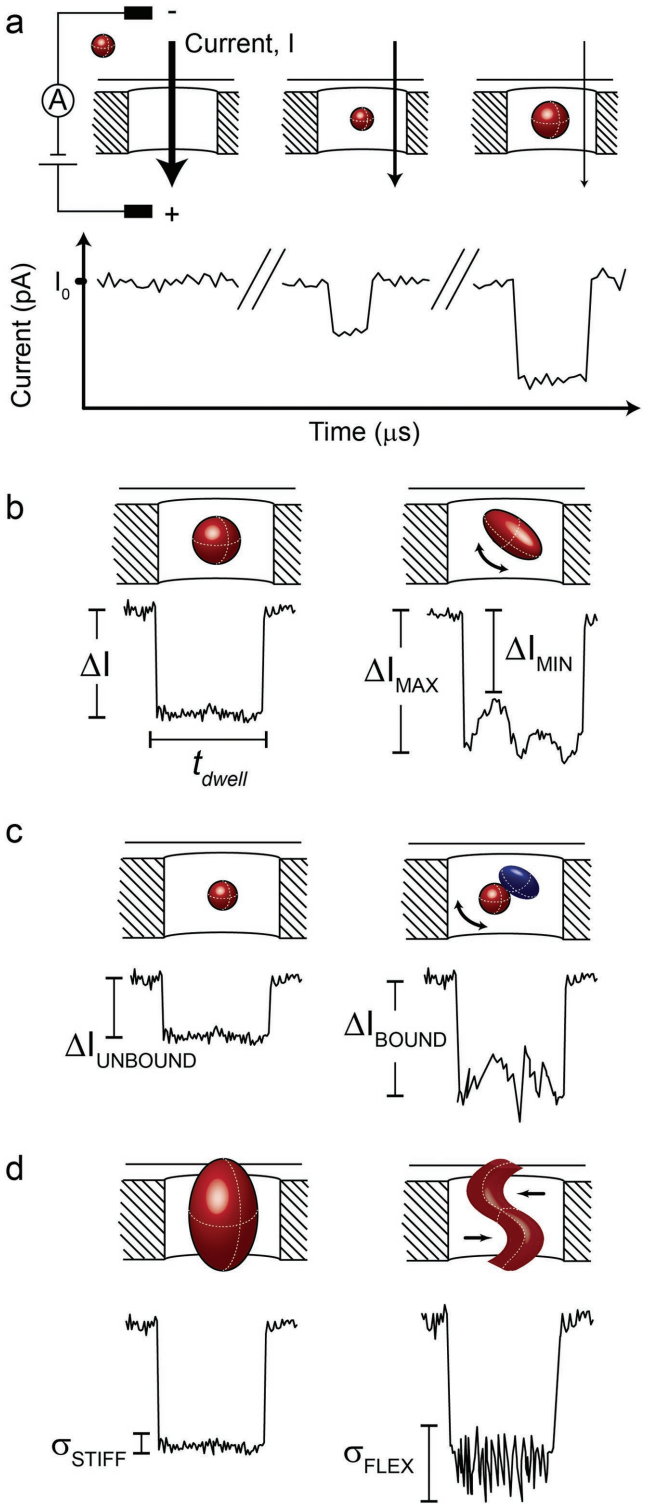

Figure 1. Cartoons relating the passage of different particles through a sensing volume to resistive pulses for particles with different volume, shape, aggregation state, or conformational flexibility. a) An electrical potential applied across the pore creates a constant ionic current, and particles passing through the sensing volume produce resistive pulses proportional to their volume. Reproduced with permission[58] U.S. Patent No. US2656508A, 1953. b) Translocation of spherical particles through cylindrical nanopores produces square-shaped resistive pulses, and the duration of translocation events is proportional to their electrophoretic mobility. Brownian rotation of nonspherical particles modulates the ionic current through the sensing volume depending on their orientation within the pore. The minimum (ΔI_{MIN}) and maximum (ΔI_{MAX}) blockade values can be used to estimate shape, dipole moment, and rotational diffusion coefficient of the particle. Reproduced with permission.[41] Copyright 2016, Macmillan Publishers Limited. c) Two or more particles bound together produce a larger resistive pulse (ΔI_{BOUND}) than sequential translocation of individual particles ($\Delta I_{UNBOUND}$). The fraction of resistive pulses from bound to unbound particles is related to binding affinities. Reproduced with permission.[76] Copyright 2006, Wiley-VCH. Reproduced with permission.[78] Copyright 2006, Elsevier B.V. d) Variations in particle structure may be revealed when confined or compressed within a sensing volume depending on the conformational stability of the molecule or molecular complexes. Less-flexible particles (σ_{STIFF}) produce resistive pulses with smaller amplitude fluctuations than flexible particles (σ_{FLEX}). Reproduced with permission.[43] Copyright 2017, American Chemical Society.

3. Amyloid Characterization with Biological Nanopores

Biological nanopores range from ion channels to assemblies of pore-forming toxins[80,81] and their biological function is to facilitate or regulate the passage of polar molecules, ions, or peptides across cell membranes.[82] With regard to resistive pulse sensing, biological nanopores are appealing as their sensing volumes are often defined with atomic precision and they can be produced in large quantities through bacteria fermentation or cell culture followed by purification.[83] Due to their extremely small sensing volumes in pore lumens with diameters smaller than 4 nm (**Figure 2**), biological nanopores are particularly well-suited to sensing small analytes, including proteins smaller than 30 kDa as well as single-stranded and double-stranded DNA or RNA.[84–86] Furthermore, several of these protein-based nanopores can be engineered by site-directed mutagenesis to integrate desired properties such as specific binding sites or residues that modify the electrostatic landscape in the pore lumen.[34,87,88]

3.1. Resistive Pulses to Interrogate Enzymatic Cleavage of Amyloid-Forming Peptides

Two key research developments facilitated the nanoscale application of resistive pulse counting with biological nanopores: inhibiting the voltage-dependent nature of ion channel proteins,[35,89,90] and limiting the rate at which biomolecules of interest transit the lumen of the pore.[91,92] These developments enabled seminal work by Bezrukov and Kasianowicz, who used the pore from α-toxin (*Staphylococcus aureus*) to measure protonation rates and to discriminate between protons and deuterons.[89,90] Kasianowicz et al. were the first to demonstrate the detection of individual polynucleotide molecules using the pore α-hemolysin,[93] and Bezrukov et al. showed that dwell times of certain polyethylene glycol (PEG) molecules were more than 1000-fold longer than values predicted by 1D diffusion because the molecules reversibly bind within the nanopore;[91] a formal theory later proposed by Lubensky and Nelson helped to explain these polymer–pore interactions.[94] This body of research established biological nanopores as resistive pulse sensors, and biological nanopores have since made it possible to detect not only polymers, but also small molecules,[61] and amyloid-forming peptides.

The first report of characterizing an amyloid-related peptide with biological nanopores focused on the amyloid-β (Aβ) peptide segment Aβ_{10-20}.[45] (Note here that Aβ refers to a peptide

© 2018 WILEY-VCH Verlag GmbH & Co. KGaA, Weinheim

Table 4. Unique attributes that make nanopore-based analyses attractive for the characterization of amyloid particles.

General to all nanopore designs
– Capability to characterize single molecules and individual molecular aggregates. This capability is an essential feature for heterogeneous amyloid particles that span a large range in aggregate diameters, lengths, and shapes and whose size and shape may determine their toxicity.
– The method isolates single particles transiently from a mixture and interrogates them one by one. This feature makes it possible to draw conclusions from an artifact-free signal that originates uniquely from the one particle under study until the particle exists the interrogation volume and makes room for the next particle.
– Method is solution-based, and therefore circumvents or reduces perturbations by drying or interactions with surfaces.
– First results are obtained within seconds after dispensing amyloid samples onto the nanopore chip therefore time-dependent changes of amyloid status may be minimized or can at least be monitored and accounted for.
– Characterization can yield rich information simultaneously from individual particles, including volume, shape, dipole moment, rotational diffusion coefficient, charge, and conformational variability of the amyloid.
– The approach is label-free making it possible to assess amyloid status without possible perturbation by labels.
– Nanopores offer one of the lowest cost and most accessible single-molecule characterization techniques. This technique is in the process of revolutionizing DNA and RNA sequencing in a broadly accessible, user-friendly, compact, and low-cost format that takes advantage of parallel recordings from hundreds of nanopores. If some of these benefits could be implemented in the context of nanopore-based amyloid analysis, then it may make longitudinal monitoring of an aging population over decades possible.
– Nanopore-based analysis requires extremely small sample volumes; microliters and even nanoliters may be sufficient. This capability may open up new strategies for sampling body fluids such as CSF that are less invasive than existing approaches.
– Analysis of experimental data from amyloid characterization can be automated and occur in real time during the translocation of individual amyloid particles through the nanopore. Amyloid status may thus be instantly updated, interpreted, and released.
– As the field progresses, atomic and molecular-scale simulations of amyloid translocations through nanopores combined with experimental and clinical data and machine learning approaches may reveal meaningful connections between the amyloid status and diagnostic and clinical significance. These developments could further strengthen and streamline analysis of amyloids and may make amyloid monitoring a routine part of medical testing.
Specific to biological nanopores
– Can detect monomers of amyloid-forming species and products of enzymatic cleavage.
– Site-directed mutagenesis of biological nanopores makes it possible to incorporate molecular groups that bind, or respond specifically, to amyloid-forming molecules.
Specific to synthetic nanopores
– Synthetic nanopore diameter and shape can, in principle, be adjusted to and optimized for various amyloid species of interest.
– Surface coatings of synthetic nanopores can bind or respond to amyloid-forming species.

involved in Alzheimer's disease that typically contains between 37 and 43 amino acids, and we denote the particular segment of Aβ using subscripted numbers.) By modifying the interior of an α-hemolysin pore to contain additional aromatic binding regions, Zhao et al. prolonged the residence times of A$\beta_{10–20}$ and other peptides rich in aromatic residues. They related residence times and resistive pulse amplitudes of the peptides to binding affinities within the nanopore, and demonstrated that nanopores could be used to determine the presence or absence of various small peptides in a mixture.[44] This setup also allowed Zhao et al. to monitor trypsin-catalyzed cleavage of A$\beta_{10–20}$. Cleavage of proteins like amyloid precursor protein (APP) by β- and γ-secretases plays a role in amyloid formation and thereby possibly influences diseases like Alzheimer's and Parkinson's.[95] These results demonstrated that nanopores can provide information about the kinetics of enzymatic cleavage of amyloids without the need to label the amyloids.[44]

3.2. Interactions between Amyloid-Forming Peptides and Molecules That Modulate Aggregation

Experiments with biological nanopores can investigate interactions between small molecules and amyloid-forming peptides. Wang et al. studied the influence of aggregation promotors like β-cyclodextrin and aggregation inhibitors like Congo red on the aggregation kinetics of Aβ. To this end, the authors followed aggregation over time by monitoring the frequencies of resistive pulses, which are related to particle concentration, and the amplitudes of resistive pulses, which are related to particle size.[46] A similar assay revealed the influence of copper (Cu^{2+}) ions on the conformation of A$\beta_{1–16}$ peptide and the rate at which it formed oligomers. Human A$\beta_{1–16}$ had stronger and longer-lasting interactions with Cu^{2+} compared to the rat variant of A$\beta_{1–16}$, likely because of a single amino acid difference (human HIS-13 vs rat ARG-13).[96] Wang et al. proposed that HIS-13 plays a role in metal-induced aggregation and could therefore be a potential therapeutic target.[97] Information about aggregation behavior of specific peptide subsequences may be useful in the context of therapeutic approaches to inhibit aggregation, and it can reveal structure–function relationships for the full-sequence peptide. For instance, the A$\beta_{25–35}$ peptide has a β-sheet structure and forms aggregates, but its inverted sequence A$\beta_{35–25}$ takes on a random coil structure and does not exhibit neurotoxicity.[98] Hu et al. found that A$\beta_{25–35}$ produced large current blockages due to its extended β-sheets and its translocation events became less frequent with time, suggesting that it was aggregating into complexes too large to enter the sensing volume of the α-hemolysin nanopore.[52] Solutions of A$\beta_{35–25}$, on the other hand, generated smaller and shorter blockage events than those of A$\beta_{25–35}$, and frequencies of A$\beta_{35–25}$ translocation events were consistent over time, suggesting that the β-sheet motif could be detected using a nanopore and likely plays a role in aggregation.[52]

© 2018 WILEY-VCH Verlag GmbH & Co. KGaA, Weinheim

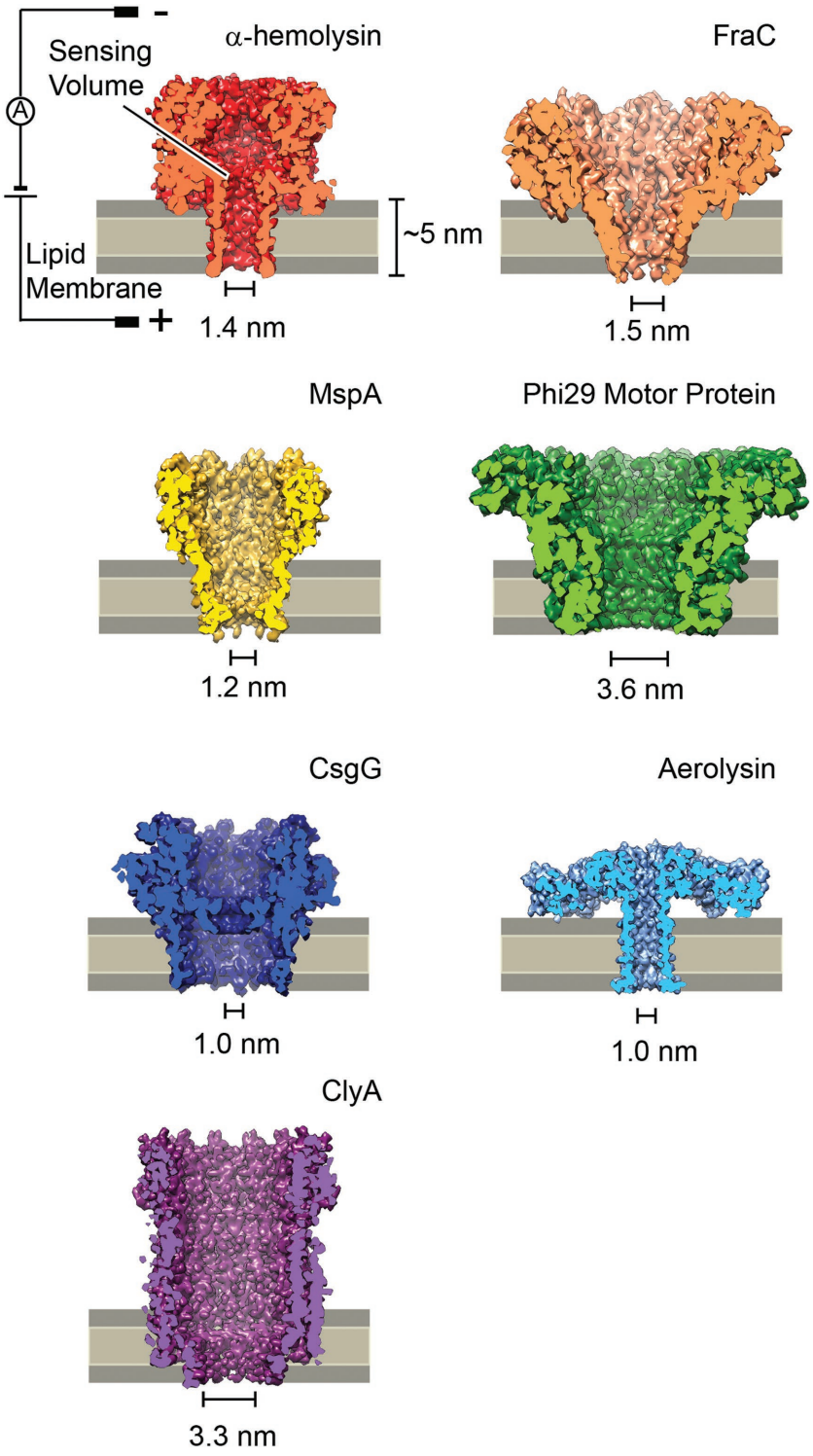

Figure 2. Cross sections of biological nanopores used in resistive pulse sensing. These illustrations show the unique high-resolution structures and sizes of these proteins, which connect two electrolyte-filled chambers across a lipid membrane. As shown for α-hemolysin, protein pores insert into lipid bilayer membranes (gray) and conduct a constant ionic current if a constant voltage is applied across the membrane. Scale bars show the narrowest constriction of each sensing volume and were measured from high-resolution structures using Chimera software with the following codes from the protein data bank: α-hemolysin (7AHL), FraC (4TSY), MspA (1UUN), Phi29 Motor Protein (1JNB), α-aerolysin (5JZT), CsgG (4UV3), and ClyA (2WCD).

3.3. Investigations of Amyloid-Forming Peptides Other Than Aβ

Most detection and characterization of amyloids with biological nanopores has focused on the Aβ peptide. As Table 1 shows, there are more than 30 amyloid-forming peptides or proteins that are associated with human disorders, including prion protein (PrP) in the spongiform encephalopathies, huntingtin protein in Huntington's disease, and α-synuclein (α-Syn) in Parkinson's disease.[5] One reason that Aβ has been popular in research with biological nanopores is its small (4.5 kDa) molecular weight; many other amyloid-forming proteins are too large in their natively folded conformation to fit through the small confines of a biological nanopore. Some proteins, like α-Syn, are natively unfolded and can pass through the nanopore as a single strand,[49] while large globular proteins can be denatured in a solution of 5 M guanidinium HCl and passed through the sensing volume in a mostly unfolded state.[47] Jeremy Lee's research group employed this denaturation strategy and reported distributions of current blockades for different prion proteins, as well as for Aβ and α-Syn.[47,99–101] Despite these approaches, the large size of some amyloid-forming proteins or their aggregates remains a major challenge to their characterization with biological pores, especially when the native structure of the protein or amyloid particle is of interest. At present, no biological pore can accommodate an intact amyloid oligomer with a diameter larger than 4 nm. Some research groups have begun to engineer protein-based nanopores with larger sizes than natural pores,[88,102,103] while others have chosen to fabricate and use synthetic nanopores in different sizes and materials.

4. Amyloid Detection and Characterization with Synthetic Nanopores

Synthetic nanopores with custom diameters in the range from 1 to 100 nm facilitate the detection and analysis of larger biomolecules including natively folded proteins[104,105] and double-stranded DNA.[106,107] Typically, these sensing volumes are fabricated by generating holes with nanometer-scale diameters in thin (less than 100 nm) insulating membranes (**Figure 3**). Manufacturing techniques for

© 2018 WILEY-VCH Verlag GmbH & Co. KGaA, Weinheim

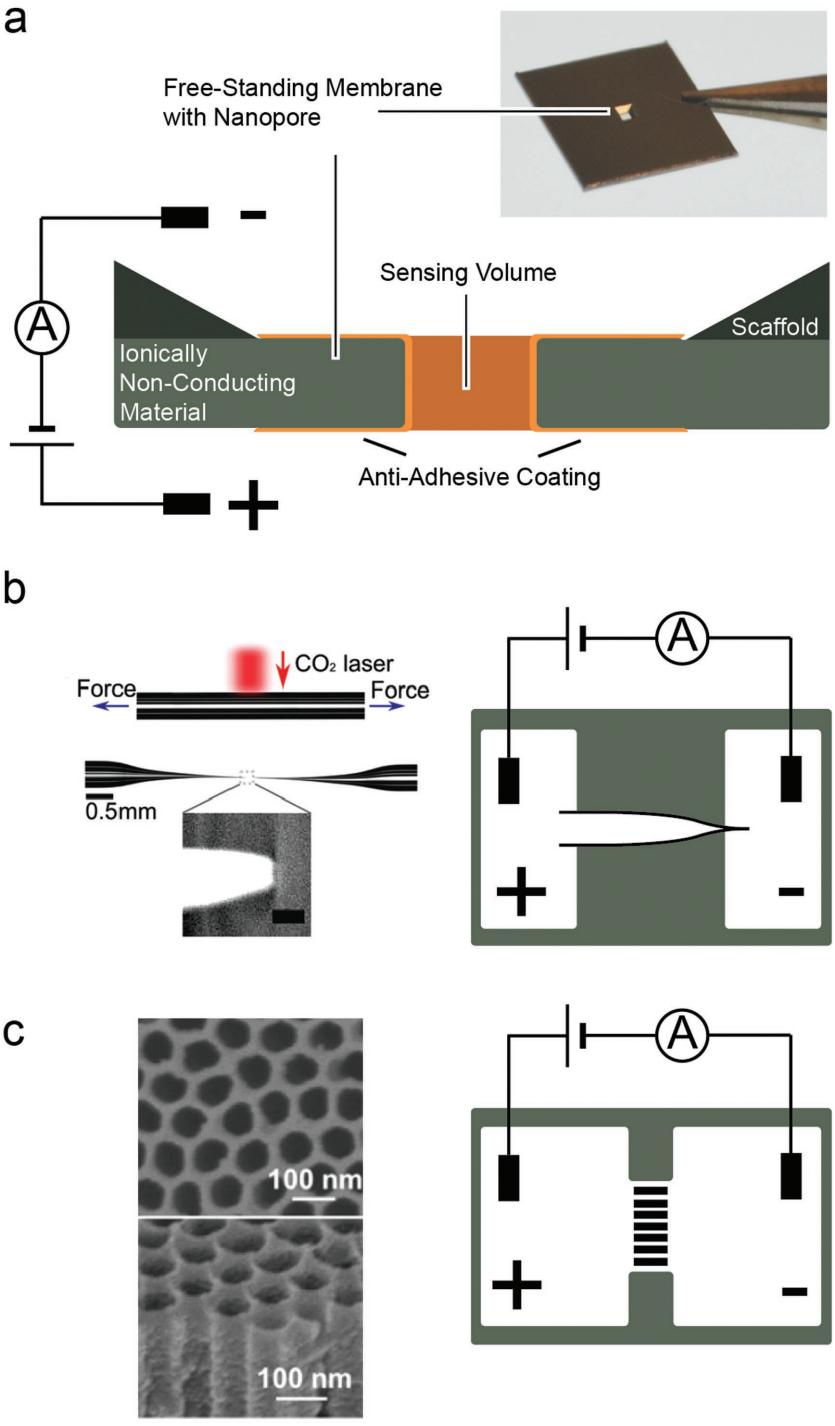

Figure 3. Schematics showing examples of synthetic nanopore designs used for amyloid characterization. a) Image of a silicon scaffold supporting a freestanding silicon nitride membrane, and cross section of a nanopore in a freestanding membrane with an antiadhesive coating. b) Glass capillary tubes can be locally heated and mechanically stretched to terminate in hollow tips with nanometer diameters. The terminal tips then act as a sensing volume that connects two electrolyte-filled reservoirs. Adapted under the terms and conditions of the Creative Commons Attribution 3.0 Unported Licence.[51] Copyright 2015, The Royal Society of Chemistry. c) Scanning electron microscopy (SEM) images of a membrane containing parallel nanochannels used to connect two reservoirs. The membrane was functionalized with amyloid-forming peptides, and the ionic current through the membrane slowly declined as peptides aggregated and occluded the channels. Adapted with permission.[54] Copyright 2016, Elsevier.

nanopore formation include dielectric breakdown,[108] TEM drilling,[109] helium ion microscope drilling,[110] capillary shrinking,[111] and gold particle heating,[112] while substrates range from silicon,[113] silica (glass),[114] silicon nitride,[105] MoS_2,[115] HfO_2,[116] and graphene.[117] Synthetic nanopores of all sizes and materials still suffer from two critical drawbacks: proteins tend to adhere to the nanopore substrate and hence clog the pore, or—when proteins do not adhere to the substrate—they transit the nanopore too quickly such that the majority of them cannot be detected by conventional electrical recording equipment.[40,118]

4.1. Lipid Bilayer Coatings Allow Measurements of Amyloids with Synthetic Nanopores

In response to these problems, several research groups in the synthetic nanopore field have focused on creating antiadhesive coatings.[40,119] One such coating introduced by our group—fluid lipid bilayers—prevents unwanted adhesion and slows protein transit through the nanopore by anchoring proteins to activated lipids.[120] To this end, we coated a silicon nitride nanopore with a supported lipid bilayer in order to characterize $A\beta_{1-40}$ peptide in the first application of a synthetic nanopore to an amyloid-related protein.[40,42] This work quantified the formation of four distinct $A\beta_{1-40}$ aggregates over the course of a 72 h aggregation period: spherical oligomers, short protofibrils, long protofibrils, and amyloid fibers. The event frequency of each species, which is a measure of their abundance, reflected the extent of aggregation; spherical oligomers gradually became less frequent as they grew in size while resistive pulses from protofibrils and mature fibers increased in frequency over time.

Coatings derived from materials other than lipid bilayers can also reduce unwanted adhesion. Rui et al. investigated α-Syn aggregation using synthetic nanopores coated with polysorbate 20 (Tween 20). This work characterized four different oligomeric species, and investigated the impact of small unilamellar vesicles (SUVs) containing certain lipids on the rates of aggregation of α-Syn.[55] Similarly, Giamblanco et al. functionalized nanopores with polyethylene glycol (PEG-5k) chains in order to study the aggregation kinetics and fibril sizes of amyloid particles comprised of lysozyme and other model proteins.[56]

© 2018 WILEY-VCH Verlag GmbH & Co. KGaA, Weinheim

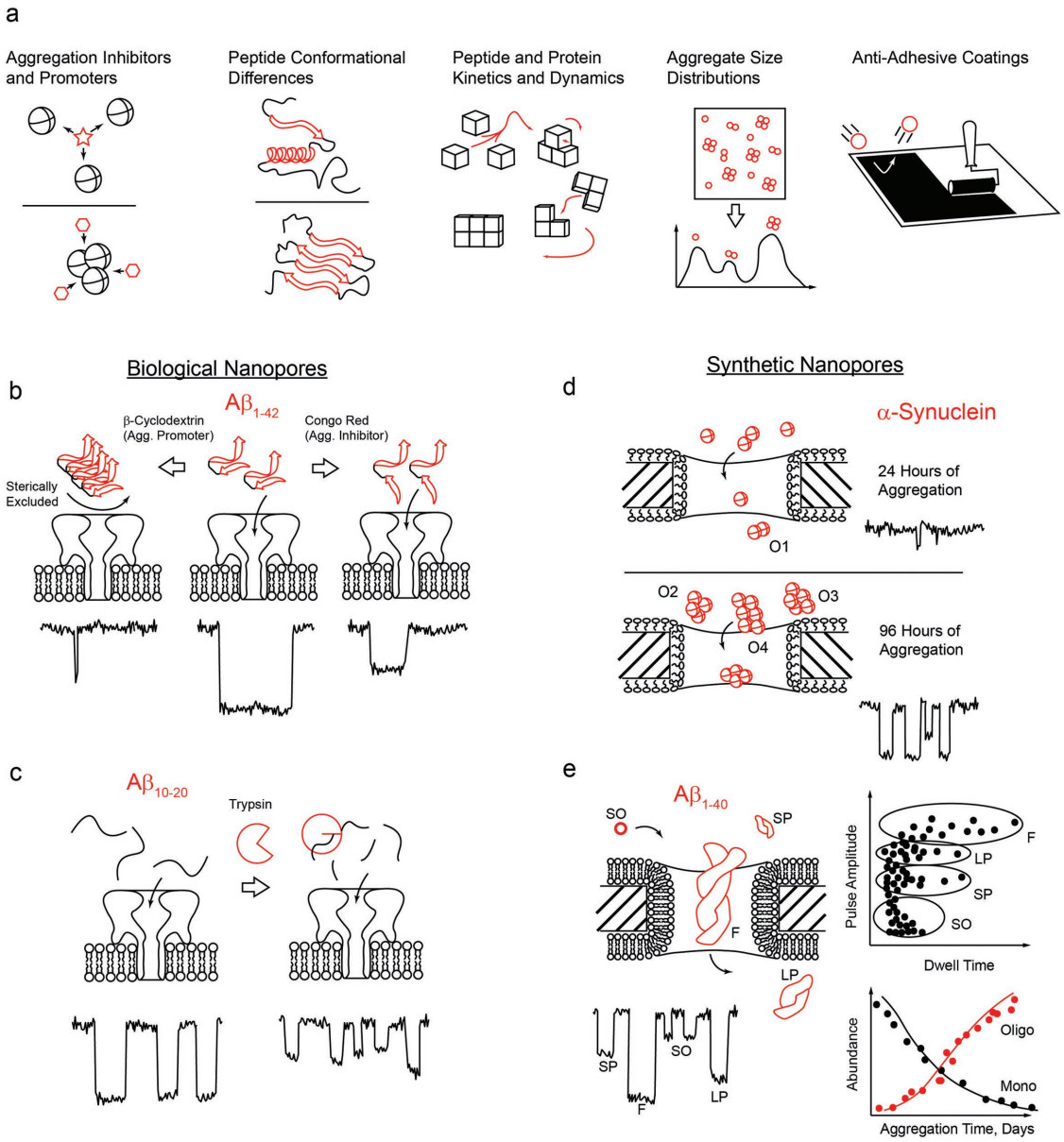

Figure 4. Cartoons summarizing various approaches for the analysis of amyloid-forming peptides with nanopores. a) Biological nanopores have been used to investigate interactions of amyloid forming peptides with aggregation promotors or inhibitors as well as to evaluate conformational differences between peptides. Synthetic nanopores have determined size distributions of aggregates over time, by employing a variety of antiadhesive coatings. Both biological and synthetic pores have been used to determine aggregation rates of amyloids. b) Amyloid beta$_{1-42}$ produces only short collision events in the presence of an aggregation promoter as the protein is sterically excluded from entering the pore, and generates small, short-lived events in the presence of an aggregation inhibitor. Adapted with permission.[46] Copyright 2011, American Chemical Society. c) As Aβ_{10-20} is enzymatically cleaved apart by trypsin, it produces smaller and shorter resistive pulses that correspond to the turnover rate and the length of the Aβ fragments. Adapted with permission.[44] Copyright 2009, American Chemical Society. d) Monitoring the formation of a-synuclein aggregates over the course of 96 h; aggregates can be grouped into four major phenotypes (O1, O2, O3, and O4). Adapted under the terms and conditions of the Creative Commons Attributions 4.0 License.[55] Copyright 2016, Macmillan Publishers Limited. e) Amyloid beta$_{(1-40)}$ undergoes a time-dependent aggregation process forming small spherical oligomers (SO), short protofibrils (SP), long protofibrils (LP), and finally mature fibrils (F) Each of these species can be detected, grouped, and characterized using a lipid bilayer coated synthetic nanopore. Adapted with permission.[42] Copyright 2012, American Chemical Society.

4.2. Model Proteins That Form Fibrils Demonstrate Assembly Processes in Nanopores

Because of difficulties with the preparation, analysis, or toxicity of amyloid samples,[26] several groups have chosen to investigate proteins like lysozyme or bovine serum albumin (BSA) that readily aggregate into amyloid-like fibrils but are not necessarily pathogenic to humans. In an attempt to develop a system that relates a population of resistive pulse amplitudes and durations to a concentration profile of amyloid (proto)fibrils, Martyushenko et al. monitored the aggregation process of lysozyme into long fibrils using glass nanocapillaries.[51] The authors performed

© 2018 WILEY-VCH Verlag GmbH & Co. KGaA, Weinheim

Table 5. Timeline of studies that characterized amyloid-forming peptides or proteins with nanopores.

Protein/peptide	Title	Nanopore style	Nanopore details	Unique aspect(s)	Year	Ref.
Amyloid-β (10–20)	Real-time monitoring of peptide cleavage using a nanopore probe	Biological	α-Hemolysin	Monitored enzymatic rate indirectly	2009	[44]
Amyloid-β (10–20)	Study of peptide transport through engineered protein channels	Biological	α-Hemolysin	Modified interior α-hemolysin nanopore to extend dwell times of peptides containing aromatic residues	2009	[45]
Amyloid-β (1–40)	Controlling protein translocation through nanopores with bioinspired fluid walls	Synthetic	Silicon nitride, lipid bilayer coated	Coated synthetic nanopores with lipid bilayers for the first time, and recorded the translocation of Aβ aggregates	2011	[40]
Amyloid-β (1–42)	Nanopore analysis of β-amyloid peptide aggregation transition induced by small molecules	Biological	α-Hemolysin	Compared aggregation kinetics of Aβ in the presence of aggregation inhibitors and promotors	2011	[46]
Amyloid-β (1–40, 1–42), α-synuclein, prion protein (PrP) human and bovine	Nanopore analysis: An emerging technique for studying the folding and misfolding of proteins	Biological	α-Hemolysin	Investigated a large group of amyloid-forming proteins with a nanopore, denatured larger proteins to fit	2012	[47]
Amyloid-β (1–40)	Single-particle characterization of Aβ oligomers in solution	Synthetic	Silicon nitride, lipid bilayer coated	Monitored the aggregation of Aβ and classified four species of aggregates	2012	[42]
Amyloid-β (1–16), human and rat	Investigation of Cu^{2+} binding to human and rat amyloid fragments Aβ (1–16) with a protein nanopore	Biological	α-Hemolysin	Related interactions between peptides and metal ions to specific amino acid differences between peptide variants	2013	[48]
α-Synuclein	Analysis of a single α-synuclein fibrillation by the interaction with a protein nanopore	Biological	α-Hemolysin	Analyzed α-synuclein with a protein nanopore, quantified aggregate-promoting interactions with lipid bilayers	2013	[49]
Prion protein (PrP)	Single protein molecule detection by glass nanopores	Synthetic	Glass nanocapillary	Compared size distribution and translocation times of PrP with other model proteins	2013	[50]
Lysozyme	Nanopore analysis of amyloid fibrils formed by lysozyme aggregation	Synthetic	Glass nanocapillary, low pH	Correlated the length of amyloid fibrils with residence times within a nanocapillary, verified results with simulations	2015	[51]
Amyloid-β (25–35, 35–25)	Single-molecule study of initial structural features on the amyloidosis process	Biological	α-Hemolysin	Observed differences in conformation and aggregation rate of two identically sized peptides	2016	[52]
Lysozyme, avidin, and IgG	Influence of adsorption on proteins and amyloid detection by silicon nitride nanopore	Synthetic	Silicon nitride, acid precleaning	In-depth analysis of the impact of adhesion on the dwell times of three amyloid-forming proteins. Correlation of blockades with monomer additions	2016	[53]
Amyloid-β (1–40)	A novel device of array nanochannels integrated electrochemical detector for detection of amyloid β aggregation and inhibitor screening	Synthetic	Nanochannel array, IR measurements	Used a parallel array of nanopores coated with Aβ to monitor the aggregation kinetics of Aβ in solution based on increased resistance	2016	[54]
α-Synuclein	Intrinsic and membrane-facilitated α-synuclein oligomerization revealed by label-free detection through solid-state nanopores	Synthetic	Silicon nitride, Tween20 coated	Measured the aggregation kinetics of α-Syn, determined four distinct oligomeric species, monitored aggregation in the presence of different lipid membranes	2016	[55]
Lysozyme, β-lactoglobulin, BSA	Detection of protein aggregate morphology through single antifouling nanopore	Synthetic	Silicon nitride, PEG-coated	Used PEG-coated pore, and incorporated ellipsoidal shape analysis to estimate fibril lengths	2018	[56]

the experiments at pH 2.0 in order to prevent adhesion to the glass substrate and determined a distribution of aggregates that they compared with results from simulations.[51] Balme et al. expanded upon this research with lysozyme fibrils and focused on the effects of protein adhesion to the surface of a silicon nitride nanopore; these authors mitigated adhesion by treating the nanopore with concentrated sulfuric acid directly before experiments. The authors then extracted distinct populations of lysozyme oligomers from the distribution of resistive pulse amplitudes and correlated those particular populations with individual monomer additions.[53]

4.3. Investigations of Prion Protein with Synthetic Nanopores

Li et al. took advantage of the large volumes of synthetic nanopores to characterize and compare a range of commonly available proteins like BSA and IgG_1 antibody as well as human PrP.[50] This report represented the first measurements of native PrP with a synthetic nanopore. The experiments were hampered by transient protein adhesion to the glass substrate, but nonetheless revealed differences in dwell times and pulse amplitudes between standard proteins and PrP; the authors related these differences to protein structure and aggregation

© 2018 WILEY-VCH Verlag GmbH & Co. KGaA, Weinheim

Table 6. Challenges of characterizing amyloid particles using nanopores, and potential solutions.

Specific challenges of characterizing amyloids with nanopores	Potential solution(s) to challenges
General to all nanopore designs	
– Distinguishing amyloid particles from other macromolecules in solution.	– Amyloid-specific binders, combined with optical techniques.
– A range of nanopore diameters is necessary to characterize the entire range of amyloid species from monomer to fiber.	– Chambers engineered for parallel electrical recordings.
– Long protofibrils and mature fibrils may not enter the pore.	– Increase size distribution of nanopores. Explore various nanopore shapes.
– High salt concentration of recording electrolytes affects aggregation kinetics of amyloid-forming peptides and proteins.	– Perform experiments at physiologic ion concentrations by reducing noise.
– Specialized technique that requires specialized instrumentation and expertise.	– Automate technique in a commercial format.
– Removal of high-abundance proteins from sample without interfering with amyloid status.	– Employ separation techniques such as affinity pull-down before analysis.
Specific to biological nanopores	
– Amyloid-forming proteins and, in particular, amyloid aggregates are too large to translocate through the biological nanopores that are currently available.	– Engineer larger biological nanopores.
– Capacitive current noise from bilayer capacitance, especially at high bandwidth.	– Minimize membrane area.
– Fragility of lipid membranes to biological samples.	– Separate chambers with a robust synthetic polymer instead of a lipid bilayer.
– Need to prepare lipid membrane before nanopore insertion.	– Employ robust preformed membranes.
– Need to reconstitute biological pore into lipid membrane.	– Preinsert biological nanopore and engineer pore to remain stable for long periods of time.
Specific to synthetic nanopores	
– Strong, nonspecific interactions with the nanopore wall can lead to artifacts in the characterization of amyloids and to clogging of the pore.	– Generate surface coatings with desired properties.
– Large current noise at high bandwidth from electrical capacitance in silicon substrates.	– Fabricate nanopores in glass (silica) or other substrates with low capacitance.
– Limited access to high-quality nanopores with desired characteristics like dimensions, geometry, surface chemistry, and amenity to surface coating.	– Improve fabrication and characterization methods for synthetic nanopores.

processes.[50] In general, synthetic nanopores enable direct monitoring of changes in the populations of oligomeric species and of large natively folded monomers (**Figure 4**). Recent years indicate a shift toward synthetic nanopores for amyloid sensing (**Table 5**), and we expect this trend to continue with the development of low-noise recording setups,[121] high-bandwidth recording equipment,[122] and advanced surface coating technologies[40,123] that may selectively bind amyloids. Because of their single-molecule sensitivity and broad size range, synthetic nanopores may ultimately provide insight into the ways in which these amyloid-forming proteins aggregate, their size distributions, and their structures.

5. Challenges and Outlook

Given the development and commercialization success of nanopore-based DNA and RNA sequencing over the past 20 years,[61,124–128] it is clear that resistive pulse sensing provides exciting opportunities as a bioanalytical method on the nanoscale. Applications of the technique to protein-based analytes, however, have not yet fully realized this potential. For example, one of the most compelling aspects of resistive pulse sensing—analyzing an individual resistive pulse to determine the physical characteristics of the unique particle that produced it—has yet to be fully exploited on amyloid targets. All of the work in Table 5 measured resistive pulses resulting from the translocations of single amyloid particles but performed subsequent analyses on populations of resistive pulses. Furthermore, these studies typically reduced resistive pulses to two quantities, amplitude and dwell time, before clustering those data into groups to generate high-level comparisons about aggregation rates and distributions of aggregate sizes. These analyses produced insights into processes of amyloid aggregation and the size of aggregates, but they overlooked rich information about relevant physical properties of individual amyloid particles such as shape, dipole moment, or conformational variability. In order to take full advantage of this detailed single-amyloid information in a way that may have clinical usefulness, nanopore sensors must first overcome several challenges summarized in **Table 6**.

Diagnostic characterization of a patient's amyloid profile with nanopores requires investigation of complex biological solutions like blood or CSF. A fundamental challenge of applying label-free single-molecule techniques to such samples is the ability to discriminate between a few analytes of interest and a large concentration of background molecules. Purification techniques like filtration, size exclusion, or affinity chromatography can remove most of these background molecules, but they prolong analyses and add complications that can limit usefulness. For instance, the presence of interfaces as well as changes in pH or ionic strength during these procedures may influence the amyloid aggregation state in the sample. Direct analysis of complex samples without purification is possible when employing target-specific detection labels.[129] Amit Meller's group simultaneously monitored optical and electrical signals of a strand of fluorescently labeled DNA transiting a

© 2018 WILEY-VCH Verlag GmbH & Co. KGaA, Weinheim

nanopore,[130] and a similar approach may allow for selective resistive pulse analyses in complex protein samples. Optical methods can even replace electrical measurements to monitor ionic current through a nanopore, as has been shown with calcium-flux sensing on nanopore arrays.[74,131–134] The challenge is, however, to collect a sufficient number of photons during the short-lived dwell times (µs) of proteins through nanopores. Solutions may emerge from sensing volumes themselves, as they can also be engineered to interact specifically with a target analyte. Binding sites designed inside or around biological nanopores enhance detection of target molecules through transient binding,[135] and synthetic nanopores with fluid lipid bilayer coatings can concentrate specific molecules around the surface of the pore by incorporating lipid anchors with binding sites into the coating.[40] But even when applying techniques to improve specificity, resistive pulse sensing with a single nanopore is still inherently a serial process and profiling the individual molecules in a unpurified mixture may require long recording times. This limitation can be addressed through parallelization as shown by Oxford Nanopore Technologies with their recent nanopore-based DNA sequencing devices that record data from hundreds of nanopores independently and simultaneously.[136] Meanwhile, novel integrated complementary metal-oxide-semiconductor (CMOS) current amplifiers combined with nanopore chips with low electrical capacitance will continue to improve the signal-to-noise ratio of high-bandwidth current recordings and provide more detailed and accurate insights from the translocations of single particles than the electrical setups currently available.[122] Fast and high-fidelity data acquisition requires robust data processing, and improvements in recording equipment have prompted a trend toward applying machine learning algorithms to resistive pulse-based data, including deep learning by neural networks.[137,138] Amyloid characterization with nanopores will also benefit from further development and optimization of sensing volumes. While biological pores are currently limited to diameters less than 4 nm, engineered protein pores[102,103] as well as DNA origami channels[139] might extend the range of potential analyte sizes. Novel coating strategies taking inspiration from nature[40,140] can overcome unwanted adhesion issues for synthetic pores, while fabrication techniques like dielectric breakdown[108] or laser-assisted nanopore formation[141] can quickly produce single-use pores without the need for sophisticated equipment.

Few, if any, techniques can quickly identify, quantify, and characterize individual unlabeled proteins or protein aggregates in a complex aqueous sample.[142] Because nanopores can probe multiple physical parameters of individual particles in solution, we suggest that they are compelling candidates for an analytical platform technology that makes it possible to detect and characterize amyloid aggregates. We hope that the studies summarized here represent the initial steps toward a rapid and robust amyloid characterization platform using nanopores. If solutions to the challenges above can be incorporated into a single device, we propose that nanopore-based single particle analysis has the potential to improve the diagnosis of neurodegenerative diseases. Ultimately, nanopore-based amyloid characterization may enable monitoring of neurodegenerative disease progression using microliter volumes of patient samples in a rapid, low-cost, and broadly accessible format that can be applied routinely and longitudinally to an ever growing and aging population. The insights gained from such population-based monitoring may help to accelerate the development of new therapies against those diseases.

Acknowledgements

This work was financially supported through the National Centre of Competence in Research *Bio-Inspired Materials*, the Adolphe Merkle Foundation, Oxford Nanopore Technologies (M.M. and J.L., Grant No. 350509-N016133), the Swiss National Science Foundation (M.M., Grant No. 200021-169304), and a Graduate Research Fellowship from the U.S. National Science Foundation (J.H.). The authors would like to thank Thomas B. H. Schroeder for thoughtful discussions and insight related to the article.

Conflict of Interest

The authors declare no conflict of interest.

Keywords

amyloid aggregate, biomarker, nanopore, resistive pulse sensing, single molecule

Received: June 24, 2018
Revised: August 15, 2018
Published online: September 17, 2018

[1] J. Hardy, D. J. Selkoe, *Science* **2002**, *297*, 353.
[2] F. Chiti, C. M. Dobson, *Annu. Rev. Biochem.* **2006**, *75*, 333.
[3] T. P. Knowles, M. J. Buehler, *Nat. Nanotechnol.* **2011**, *6*, 469.
[4] C. Haass, D. J. Selkoe, *Nat. Rev. Mol. Cell Biol.* **2007**, *8*, 101.
[5] D. Eisenberg, M. Jucker, *Cell* **2012**, *148*, 1188.
[6] C. Ballard, S. Gauthier, A. Corbett, C. Brayne, D. Aarsland, E. Jones, *Lancet* **2011**, *377*, 1019.
[7] World Health Organization, *Dementia: A Public Health Priority*, World Health Organization, **2012**.
[8] J. J. Yerbury, L. Ooi, A. Dillin, D. N. Saunders, D. M. Hatters, P. M. Beart, N. R. Cashman, M. R. Wilson, H. Ecroyd, *J. Neurochem.* **2016**, *137*, 489.
[9] T. L. Spires-Jones, J. Attems, D. R. Thal, *Acta Neuropathol.* **2017**, *134*, 187.
[10] R. Nelson, M. R. Sawaya, M. Balbirnie, A. Ø. Madsen, C. Riekel, R. Grothe, D. Eisenberg, *Nature* **2005**, *435*, 773.
[11] J. T. Jarrett, P. T. Lansbury Jr., *Cell* **1993**, *73*, 1055.
[12] X. Han, G. He, *ACS Chem. Neurosci.* **2018**, *9*, 198.
[13] P. Prangkio, E. C. Yusko, D. Sept, J. Yang, M. Mayer, *PLoS One* **2012**, *7*, e47261.
[14] S. Pellegrino, N. Tonali, E. Erba, J. Kaffy, M. Taverna, A. Contini, M. Taylor, D. Allsop, M. L. Gelmi, S. Ongeri, *Chem. Sci.* **2017**, *8*, 1295.
[15] M. Hölttä, O. Hansson, U. Andreasson, J. Hertze, L. Minthon, K. Nägga, N. Andreasen, H. Zetterberg, K. Blennow, *PLoS One* **2013**, *8*, e66381.
[16] O. Hansson, S. Hall, A. Öhrfelt, H. Zetterberg, K. Blennow, L. Minthon, K. Nägga, E. Londos, S. Varghese, N. K. Majbour, *Alzheimer's Res. Ther.* **2014**, *6*, 25.
[17] E. Bagyinszky, V. Van Giau, K. Shim, K. Suk, S. S. A. An, S. Kim, *J. Neurol. Sci.* **2017**, *376*, 242.

 © 2018 WILEY-VCH Verlag GmbH & Co. KGaA, Weinheim

[18] B. Olsson, R. Lautner, U. Andreasson, A. Öhrfelt, E. Portelius, M. Bjerke, M. Hölttä, C. Rosén, C. Olsson, G. Strobel, *Lancet Neurol.* **2016**, *15*, 673.
[19] S. J. C. Lee, E. Nam, H. J. Lee, M. G. Savelieff, M. H. Lim, *Chem. Soc. Rev.* **2017**, *46*, 310.
[20] H. Li, F. Rahimi, S. Sinha, P. Maiti, G. Bitan, K. Murakami, *Encyclopedia of Analytical Chemistry: Applications, Theory and Instrumentation*, John Wiley & Sons Ltd., Chichester, UK **2006**.
[21] D. B. Teplow, N. D. Lazo, G. Bitan, S. Bernstein, T. Wyttenbach, M. T. Bowers, A. Baumketner, J.-E. Shea, B. Urbanc, L. Cruz, *Acc. Chem. Res.* **2006**, *39*, 635.
[22] M. R. Nilsson, *Methods* **2004**, *34*, 151.
[23] F. Chiti, C. M. Dobson, *Annu. Rev. Biochem.* **2017**, *86*, 27.
[24] A. E. Langkilde, B. Vestergaard, *FEBS Lett.* **2009**, *583*, 2600.
[25] S. W. Chen, S. Drakulic, E. Deas, M. Ouberai, F. A. Aprile, R. Arranz, S. Ness, C. Roodveldt, T. Guilliams, E. J. De-Genst, *Proc. Natl. Acad. Sci. USA* **2015**, *112*, E1994.
[26] M. G. Zagorski, J. Yang, H. Shao, K. Ma, H. Zeng, A. Hong, *Methods in Enzymology*, Academic, San Diego, CA **1999**, pp. 189–204.
[27] B. J. Alper, W. K. Schmidt, *J. Neurosci. Methods* **2009**, *178*, 40.
[28] C. G. Glabe, *J. Biol. Chem.* **2008**, *283*, 29639.
[29] A. N. Klein, T. Ziehm, T. van Groen, I. Kadish, A. Elfgen, M. Tusche, M. Thomaier, K. Reiss, O. Brener, L. Gremer, *ACS Chem. Neurosci.* **2017**, *8*, 1889.
[30] V. L. Villemagne, V. Doré, S. C. Burnham, C. L. Masters, C. C. Rowe, *Nat. Rev. Neurol.* **2018**, *14*, 225.
[31] R. W. DeBlois, C. P. Bean, *Rev. Sci. Instrum.* **1970**, *41*, 909.
[32] H. Bayley, C. R. Martin, *Chem. Rev.* **2000**, *100*, 2575.
[33] C. D. Ahrberg, J. M. Lee, B. G. Chung, *Sci. Rep.* **2018**, *8*, 2438.
[34] L.-Q. Gu, O. Braha, S. Conlan, S. Cheley, H. Bayley, *Nature* **1999**, *398*, 686.
[35] J. J. Kasianowicz, A. K. Balijepalli, J. Ettedgui, J. H. Forstater, H. Wang, H. Zhang, J. W. Robertson, *Biochim. Biophys. Acta, Biomembr.* **2016**, *1858*, 593.
[36] M. Ali, S. Nasir, Q. H. Nguyen, J. K. Sahoo, M. N. Tahir, W. Tremel, W. Ensinger, *J. Am. Chem. Soc.* **2011**, *133*, 17307.
[37] W. Shi, A. K. Friedman, L. A. Baker, *Anal. Chem.* **2017**, *89*, 157.
[38] W.-J. Lan, D. A. Holden, B. Zhang, H. S. White, *Anal. Chem.* **2011**, *83*, 3840.
[39] R. Vogel, W. Anderson, J. Eldridge, B. Glossop, G. Willmott, *Anal. Chem.* **2012**, *84*, 3125.
[40] E. C. Yusko, J. M. Johnson, S. Majd, P. Prangkio, R. C. Rollings, J. Li, J. Yang, M. Mayer, *Nat. Nanotechnol.* **2011**, *6*, 253.
[41] E. C. Yusko, B. R. Bruhn, O. M. Eggenberger, J. Houghtaling, R. C. Rollings, N. C. Walsh, S. Nandivada, M. Pindrus, A. R. Hall, D. Sept, J. Li, D. S. Kalonia, M. Mayer, *Nat. Nanotechnol.* **2017**, *12*, 360.
[42] E. C. Yusko, P. Prangkio, D. Sept, R. C. Rollings, J. Li, M. Mayer, *ACS Nano* **2012**, *6*, 5909.
[43] P. Waduge, R. Hu, P. Bandarkar, H. Yamazaki, B. Cressiot, Q. Zhao, P. C. Whitford, M. Wanunu, *ACS Nano* **2017**, *11*, 5706.
[44] Q. Zhao, R. S. S. de Zoysa, D. Wang, D. A. Jayawardhana, X. Guan, *J. Am. Chem. Soc.* **2009**, *131*, 6324.
[45] Q. Zhao, D. A. Jayawardhana, D. Wang, X. Guan, *J. Phys. Chem. B* **2009**, *113*, 3572.
[46] H.-Y. Wang, Y.-L. Ying, Y. Li, H.-B. Kraatz, Y.-T. Long, *Anal. Chem.* **2011**, *83*, 1746.
[47] C. A. Madampage, O. Tavassoly, C. Christensen, M. Kumari, J. S. Lee, *Prion* **2012**, *6*, 116.
[48] A. Asandei, I. Schiopu, S. Iftemi, L. Mereuta, T. Luchian, *Langmuir* **2013**, *29*, 15634.
[49] H.-Y. Wang, Z. Gu, C. Cao, J. Wang, Y.-T. Long, *Anal. Chem.* **2013**, *85*, 8254.
[50] W. Li, N. A. Bell, S. Hernández-Ainsa, V. V. Thacker, A. M. Thackray, R. Bujdoso, U. F. Keyser, *ACS Nano* **2013**, *7*, 4129.
[51] N. Martyushenko, N. A. Bell, R. D. Lamboll, U. F. Keyser, *Analyst* **2015**, *140*, 4882.
[52] Y.-X. Hu, Y.-L. Ying, Z. Gu, C. Cao, B.-Y. Yan, H.-F. Wang, Y.-T. Long, *Chem. Commun.* **2016**, *52*, 5542.
[53] S. Balme, P. E. Coulon, M. Lepoitevin, B. Charlot, N. Yandrapalli, C. Favard, D. Muriaux, M. Bechelany, J.-M. Janot, *Langmuir* **2016**, *32*, 8916.
[54] C. Wang, H.-L. Liu, Y.-Q. Li, J. Cao, B. Zheng, X.-H. Xia, F. Feng, *Electrochem. Commun.* **2016**, *66*, 25.
[55] R. Hu, J. Diao, J. Li, Z. Tang, X. Li, J. Leitz, J. Long, J. Liu, D. Yu, Q. Zhao, *Sci. Rep.* **2016**, *6*, 20776.
[56] N. Giamblanco, D. Coglitore, J.-M. Janot, P. E. Coulon, B. Charlot, S. Balme, *Sens. Actuators, B* **2018**, *260*, 736.
[57] V. Sauvage, L. Boizeau, D. Candotti, M. Vandenbogaert, A. Servant-Delmas, V. Caro, S. Laperche, *PLoS One* **2018**, *13*, e0194366.
[58] W. H. Coulter, U.S Patent, US2656508A, **1953**.
[59] D. S. Talaga, J. Li, *J. Am. Chem. Soc.* **2009**, *131*, 9287.
[60] K. J. Freedman, M. Jürgens, A. Prabhu, C. W. Ahn, P. Jemth, J. B. Edel, M. J. Kim, *Anal. Chem.* **2011**, *83*, 5137.
[61] J. W. Robertson, C. G. Rodrigues, V. M. Stanford, K. A. Rubinson, O. V. Krasilnikov, J. J. Kasianowicz, *Proc. Natl. Acad. Sci. USA* **2007**, *104*, 8207.
[62] F. Haque, J. Li, H.-C. Wu, X.-J. Liang, P. Guo, *Nano Today* **2013**, *8*, 56.
[63] M. Wanunu, *Phys. Life Rev.* **2012**, *9*, 125.
[64] B. M. Venkatesan, R. Bashir, *Nat. Nanotechnol.* **2011**, *6*, 615.
[65] H. P. J. Buermans, J. T. Den Dunnen, *Biochim. Biophys. Acta,– Mol. Basis Dis.* **2014**, *1842*, 1932.
[66] S. Howorka, Z. Siwy, *Chem. Soc. Rev.* **2009**, *38*, 2360.
[67] D. Branton, D. W. Deamer, A. Marziali, H. Bayley, S. A. Benner, T. Butler, M. Di Ventra, S. Garaj, A. Hibbs, X. Huang, S. B. Jovanovich, P. S. Krstic, S. Lindsay, X. S. Ling, C. H. Mastrangelo, A. Meller, J. S. Oliver, Y. V. Pershin, J. M. Ramsey, R. Riehn, G. V. Soni, V. Tabard-Cossa, M. Wanunu, M. Wiggin, J. A. Schloss, *Nat. Biotechnol.* **2008**, *26*, 1146.
[68] D. C. Golibersuch, *Biophys. J.* **1973**, *13*, 265.
[69] J. J. Kasianowicz, S. E. Henrickson, H. H. Weetall, B. Robertson, *Anal. Chem.* **2001**, *73*, 2268.
[70] W. R. Smythe, *Phys. Fluids* **1964**, *7*, 633.
[71] H. Fricke, *J. Appl. Phys.* **1953**, *24*, 644.
[72] S. Velick, M. Gorin, *J. Gen. Physiol.* **1940**, *23*, 753.
[73] M. Mayer, E. Yusko, *Google Patents*, **2017**.
[74] A. Ivankin, S. Carson, S. R. Kinney, M. Wanunu, *J. Am. Chem. Soc.* **2013**, *135*, 15350.
[75] M. Langecker, A. Ivankin, S. Carson, S. R. Kinney, F. C. Simmel, M. Wanunu, *Nano Lett.* **2015**, *15*, 783.
[76] J. D. Uram, K. Ke, A. J. Hunt, M. Mayer, *Small* **2006**, *2*, 967.
[77] J. D. Uram, K. Ke, A. J. Hunt, M. Mayer, *Angew. Chem., Int. Ed.* **2006**, *45*, 2281.
[78] J. D. Uram, M. Mayer, *Biosens. Bioelectron.* **2007**, *22*, 1556.
[79] W. Si, A. Aksimentiev, *ACS Nano* **2017**, *11*, 7091.
[80] M. D. Peraro, F. G. van der Goot, *Nat. Rev. Microbiol.* **2016**, *14*, 77.
[81] A. Fennouri, S. F. Mayer, T. B. H. Schroeder, M. Mayer, *Biochim. Biophys. Acta, Biomembr.* **2017**, *1859*, 2051.
[82] J. Zlatanova, K. van Holde, *Mol. Cell* **2006**, *24*, 317.
[83] A. L. Demain, P. Vaishnav, *Biotechnol. Adv.* **2009**, *27*, 297.
[84] G. Huang, K. Willems, M. Soskine, C. Wloka, G. Maglia, *Nat. Commun.* **2017**, *8*, 935.
[85] C. Wloka, V. Van Meervelt, D. van Gelder, N. Danda, N. Jager, C. P. Williams, G. Maglia, *ACS Nano* **2017**, *11*, 4387.
[86] D. Wendell, P. Jing, J. Geng, V. Subramaniam, T. J. Lee, C. Montemagno, P. Guo, *Nat. Nanotechnol.* **2009**, *4*, 765.
[87] S. Howorka, S. Cheley, H. Bayley, *Nat. Biotechnol.* **2001**, *19*, 636.
[88] M. Soskine, A. Biesemans, M. De Maeyer, G. Maglia, *J. Am. Chem. Soc.* **2013**, *135*, 13456.

© 2018 WILEY-VCH Verlag GmbH & Co. KGaA, Weinheim

[89] S. M. Bezrukov, J. J. Kasianowicz, *Phys. Rev. Lett.* **1993**, *70*, 2352.
[90] J. J. Kasianowicz, S. M. Bezrukov, *Biophys. J.* **1995**, *69*, 94.
[91] S. M. Bezrukov, I. Vodyanoy, R. A. Brutyan, J. J. Kasianowicz, *Macromolecules* **1996**, *29*, 8517.
[92] J. J. Kasianowicz, J. W. F. Robertson, E. R. Chan, J. E. Reiner, V. M. Stanford, *Annu. Rev. Anal. Chem.* **2008**, *1*, 737.
[93] J. J. Kasianowicz, E. Brandin, D. Branton, D. W. Deamer, *Proc. Natl. Acad. Sci. USA* **1996**, *93*, 13770.
[94] D. K. Lubensky, D. R. Nelson, *Biophys. J.* **1999**, *77*, 1824.
[95] R. A. Sharples, L. J. Vella, R. M. Nisbet, R. Naylor, K. Perez, K. J. Barnham, C. L. Masters, A. F. Hill, *FASEB J.* **2008**, *22*, 1469.
[96] L. Hong, T. M. Carducci, W. D. Bush, C. G. Dudzik, G. L. Millhauser, J. D. Simon, *J. Phys. Chem. B* **2010**, *114*, 11261.
[97] C. C. Curtain, F. E. Ali, D. G. Smith, A. I. Bush, C. L. Masters, K. J. Barnham, *J. Biol. Chem.* **2003**, *278*, 2977.
[98] G. Olivieri, G. Baysang, F. Meier, F. Müller-Spahn, H. B. Stähelin, M. Brockhaus, C. H. Brack, *J. Neurochem.* **2001**, *76*, 224.
[99] R. I. Stefureac, C. A. Madampage, O. Andrievskaia, J. S. Lee, *Biochem. Cell Biol.* **2010**, *88*, 347.
[100] O. Tavassoly, J. S. Lee, *FEBS Lett.* **2012**, *586*, 3222.
[101] O. Tavassoly, J. Kakish, S. Nokhrin, O. Dmitriev, J. S. Lee, *Eur. J. Med. Chem.* **2014**, *88*, 42.
[102] A. Henning-Knechtel, J. Knechtel, M. Magzoub, *Nucleic Acids Res.* **2017**, *45*, 12057.
[103] E. Spruijt, S. E. Tusk, H. Bayley, *Nat. Nanotechnol.* **2018**, *13*, 739.
[104] A. Oukhaled, B. Cressiot, L. Bacri, M. Pastoriza-Gallego, J.-M. Betton, E. Bourhis, R. Jede, J. Gierak, L. Auvray, J. Pelta, *ACS Nano* **2011**, *5*, 3628.
[105] J. Li, D. Stein, C. McMullan, D. Branton, M. J. Aziz, J. A. Golovchenko, *Nature* **2001**, *412*, 166.
[106] J. Li, M. Gershow, D. Stein, E. Brandin, J. A. Golovchenko, *Nat. Mater.* **2003**, *2*, 611.
[107] A. Han, G. Schürmann, G. Mondin, R. A. Bitterli, N. G. Hegelbach, N. F. de Rooij, U. Staufer, *Appl. Phys. Lett.* **2006**, *88*, 093901.
[108] H. Kwok, K. Briggs, V. Tabard-Cossa, *PLoS One* **2014**, *9*, e92880.
[109] A. J. Storm, J. H. Chen, X. S. Ling, H. W. Zandbergen, C. Dekker, *Nat. Mater.* **2003**, *2*, 537.
[110] J. Yang, D. C. Ferranti, L. A. Stern, C. A. Sanford, J. Huang, Z. Ren, L.-C. Qin, A. R. Hall, *Nanotechnology* **2011**, *22*, 285310.
[111] L. J. Steinbock, J. F. Steinbock, A. Radenovic, *Nano Lett.* **2013**, *13*, 1717.
[112] L. J. de Vreede, A. van den Berg, J. C. Eijkel, *Nano Lett.* **2015**, *15*, 727.
[113] J. B. Heng, V. Dimitrov, Y. V. Grinkova, C. Ho, T. Kim, D. Muller, S. Sligar, T. Sorsch, R. Twesten, R. Timp, G. Timp, *IEEE Int. Electron Devices Meet.* **2003**, 32.2.1.
[114] M.-H. Lee, A. Kumar, K.-B. Park, S.-Y. Cho, H.-M. Kim, M.-C. Lim, Y.-R. Kim, K.-B. Kim, *Sci. Rep.* **2015**, *4*, 7448.
[115] A. B. Farimani, K. Min, N. R. Aluru, *ACS Nano* **2014**, *8*, 7914.
[116] J. Larkin, R. Henley, D. C. Bell, T. Cohen-Karni, J. K. Rosenstein, M. Wanunu, *ACS Nano* **2013**, *7*, 10121.
[117] Z. S. Siwy, M. Davenport, *Nat. Nanotechnol.* **2010**, *5*, 697.
[118] C. Plesa, S. W. Kowalczyk, R. Zinsmeester, A. Y. Grosberg, Y. Rabin, C. Dekker, *Nano Lett.* **2013**, *13*, 658.
[119] L. T. Sexton, H. Mukaibo, P. Katira, H. Hess, S. A. Sherrill, L. P. Horne, C. R. Martin, *J. Am. Chem. Soc.* **2010**, *132*, 6755.
[120] M. Mayer, E. Yusko, J. Yang, *Google Patents*, **2016**.
[121] A. Balan, C.-C. Chien, R. Engelke, M. Drndić, *Sci. Rep.* **2016**, *5*, 17775.
[122] J. K. Rosenstein, M. Wanunu, C. A. Merchant, M. Drndic, K. L. Shepard, *Nat. Methods* **2012**, *9*, 487.
[123] A. Ananth, M. Genua, N. Aissaoui, L. Díaz, N. B. Eisele, S. Frey, C. Dekker, R. P. Richter, D. Görlich, *Small* **2018**, *14*, 1703357.
[124] E. A. Manrao, I. M. Derrington, A. H. Laszlo, K. W. Langford, M. K. Hopper, N. Gillgren, M. Pavlenok, M. Niederweis, J. H. Gundlach, *Nat. Biotechnol.* **2012**, *30*, 349.
[125] A. S. Mikheyev, M. M. Tin, *Mol. Ecol. Resour.* **2014**, *14*, 1097.
[126] J. E. Reiner, J. J. Kasianowicz, B. J. Nablo, J. W. F. Robertson, *Proc. Natl. Acad. Sci. USA* **2010**, *107*, 12080.
[127] S. Kumar, C. Tao, M. Chien, B. Hellner, A. Balijepalli, J. W. F. Robertson, Z. Li, J. J. Russo, J. E. Reiner, J. J. Kasianowicz, J. Ju, *Sci. Rep.* **2012**, *2*, 684.
[128] C. W. Fuller, S. Kumar, M. Porel, M. Chien, A. Bibillo, P. B. Stranges, M. Dorwart, C. Tao, Z. Li, W. Guo, S. Shi, D. Korenblum, A. Trans, A. Aguirre, E. Liu, E. T. Harada, J. Pollard, A. Bhat, C. Cech, A. Yang, C. Arnold, M. Palla, J. Hovis, R. Chen, I. Morozova, S. Kalachikov, J. J. Russo, J. J. Kasianowicz, R. Davis, S. Roever, G. M. Church, J. Ju, *Proc. Natl. Acad. Sci. USA* **2016**, *113*, 5233.
[129] E. E. Nesterov, J. Skoch, B. T. Hyman, W. E. Klunk, B. J. Bacskai, T. M. Swager, *Angew. Chem., Int. Ed.* **2005**, *44*, 5452.
[130] G. V. Soni, A. Singer, Z. Yu, Y. Sun, B. McNally, A. Meller, *Rev. Sci. Instrum.* **2010**, *81*, 014301.
[131] S. Liu, A. R. Hawkins, H. Schmidt, *Microchim. Acta* **2016**, *183*, 1275.
[132] S. Huang, M. Romero-Ruiz, O. K. Castell, H. Bayley, M. I. Wallace, *Nat. Nanotechnol.* **2015**, *10*, 986.
[133] B. N. Anderson, O. N. Assad, T. Gilboa, A. H. Squires, D. Bar, A. Meller, *ACS Nano* **2014**, *8*, 11836.
[134] T. Gilboa, A. Meller, *Analyst* **2015**, *140*, 4733.
[135] S. Krishnan, D. Ziegler, V. Arnaut, T. G. Martin, K. Kapsner, K. Henneberg, A. R. Bausch, H. Dietz, F. C. Simmel, *Nat. Commun.* **2016**, *7*, 12787.
[136] T. Tucker, M. Marra, J. M. Friedman, *Am. J. Hum. Genet.* **2009**, *85*, 142.
[137] K. Misiunas, N. Ermann, U. F. Keyser, *Nano Lett.* **2018**.
[138] R. Y. Henley, B. A. Ashcroft, I. Farrell, B. S. Cooperman, S. M. Lindsay, M. Wanunu, *Nano Lett.* **2016**, *16*, 138.
[139] M. Langecker, V. Arnaut, T. G. Martin, J. List, S. Renner, M. Mayer, H. Dietz, F. C. Simmel, *Science* **2012**, *338*, 932.
[140] T. B. Schroeder, J. Houghtaling, B. D. Wilts, M. Mayer, *Adv. Mater.* **2018**, *30*, 1705322.
[141] R. An, J. D. Uram, E. C. Yusko, K. Ke, M. Mayer, A. J. Hunt, *Opt. Lett.* **2008**, *33*, 1153.
[142] A. E. Herr, *Anal. Chem.* **2013**, *85*, 7622.

© 2018 WILEY-VCH Verlag GmbH & Co. KGaA, Weinheim